Journal of Sol-Gel Science and Technology (2021) 99:275–283
https://doi.org/10.1007/s10971-021-05581-3

REVIEW PAPER: NANO-STRUCTURED MATERIALS (PARTICLES, FIBERS, COLLOIDS, COMPOSITES, ETC.)

Preparation and characterization of $(Zr_{0.8},Sn_{0.2})TiO_4$ nano crystals by hydrothermal-molten salt method

Qi Wu[1] · Xiangchun Liu[1] · Zhengguang Li[1] · Li Qiang[1] · Ningna Bai[1] · Kai Zhang[1] · Zhe Yang[1]

Received: 27 January 2021 / Accepted: 21 June 2021 / Published online: 8 July 2021

Abstract

The pure phase $(Zr_{0.8},Sn_{0.2})TiO_4$ nano crystals have been prepared by hydrothermal-molten salt method. The effects of the pH of solvent system, the calcinations temperature and the ratio of composite molten salt on the phase composition and crystalline morphology have been investigated. The results show that the high pure phase $(Zr_{0.8},Sn_{0.2})TiO_4$ nano crystals with regular morphology were prepared at 1000 °C in NaCl-KCl salt system. The synthesized temperature of single phase $(Zr_{0.8},Sn_{0.2})TiO_4$ is lower and the crystal growth is more complete compared with the hydrothermal-solid state method. The rod-like crystalline grain are evenly distributed with a diameter of about 50–60 nm and can be used as start materials for preparing ZST textured ceramics. The $(Zr_{0.8},Sn_{0.2})TiO_4$ nano crystal has a certain photocatalytic effect and good UV shielding performance.

Graphical Abstract

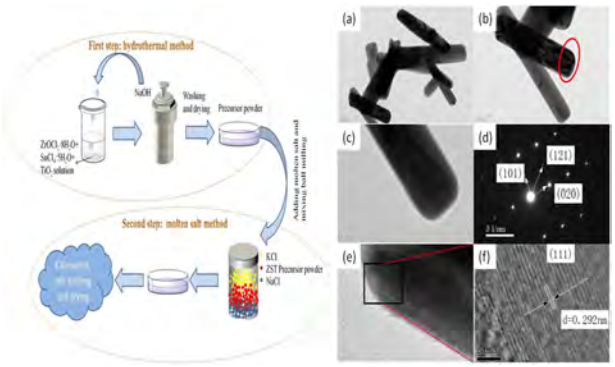

Keywords $(Zr_{0.8},Sn_{0.2})TiO_4$ · Hydrothermal · Molten salt method · Low temperature sintering

Highlights

- $(Zr_{0.8},Sn_{0.2})TiO_4$ nano powders were prepared by hydrothermal-molten salt method.
- Synthetic nano powder can be used as the starting material for preparing ZST textured ceramics.
- The synthesized powder has a certain degree of photocatalysis and good UV shielding performance.
- The synthesized powder is rod-like crystal grains, uniformly distributed, with a diameter of about 50–60 nm.

1 Introduction

With the rapid development of wireless communication technologies, such as mobile phones, satellite communication systems and global positioning systems, the demand for

✉ Xiangchun Liu
liuxc_xust@163.com

[1] Department of Materials Science and Engineering, Xi'an University of Science and Technology, Xi'an 710054, China

high-quality microwave ceramic components have increased [1–4]. Requirements for high performance microwave dielectric materials must combine with a large dielectric constant (ε_r), a high quality factor ($Q \times f$) and a near zero temperature coefficient of resonant frequency(τ_f) [5–8].

(Zr,Sn)TiO_4 ceramics, which are one of the most popular dielectric matericals for titanate microwave ceramics [9–11], have an α-PbO_2 orthorhombic structure, possessing excellent dielectric properties of moderate dielectric constant (ε_r), high quality factor ($Q \times f$), and near zero temperature coefficient of resonant frequency (τ_f) [12–14]. It is well known that ($Zr_{0.8}$,$Sn_{0.2}$)TiO_4 (abbreviated to ZST) is limited for commerical application owing to their sintering temperature as high as 1600 °C [15, 16]. Many researches have been conducted to improve the sinterability and lower the sintering temperature by using different types of dopants [17–19]. Studies have shown that the addition of dopants may give an advise affect to the dielectric properties of ZST ceramics [20–22]. Thus, it is significant to start research on reducing the particle size of the pre-synthesized powders and increasing its surface activity. Extensive researchers made effort in studying the synthesis of ZST nano powders. Haigang Yu et al. [23] successfully prepared ZST powders by adjusting the pH value at 1260 °C by hydrothermal method. Jianqiang Wu et al. [24] used the co-precipitation method to prepare nano ZnO coated SnO_2 powders as the raw material for the synthesis of ZST powders, and then mixed with other raw materials to synthesize ($Zr_{0.8}$,$Sn_{0.2}$)TiO_4 ceramics at 1260 °C by the solid phase method. Ho et al. [25] used different tin sources ($SnCl_4{\cdot}5H_2O$ and Sn$(OC_4H_9)_4$) to prepare ZST nano powders at low temperature by sol-gel method. It is found that the use of a single hydrothermal method and co-precipitation method can reduce the calcination temperature compared with the traditional solid state method, while the calcination temperature still remained as high as 1260 °C from the above research. The sol-gel method can synthesize ZST nano powders at low temperatures, but this method needs complex instrumentation and expensive raw materials [26]. Therefore, it is very necessary in preparation method to explore the new route to synthesize ZST nano powders.

In the early stage, we used different solvents to explore the synthesis of ZST powders by hydrothermal method. The results indicate that no ZST phase appeared in the samples synthesized by other solvents. While small amounts of ZST phase can be detected in the samples synthesized with water as solvent, but the main crystal phases were TiO_2 (anatase phase) and ZrO_2 phase. Therefore, a new process route named hydrothermal-solid state method was used to synthesize the ZST phase. According to the hydrothermal-solid state method, first, the precursor powders are synthesized by hydrothermal method, then the precursor powders are calcined in solid-state ambient atmospheres. The results show that ZST powders can be synthesized successfully by hydrothermal-solid state method, but there were impurities in the samples and the synthesized temperature was as high as 1100 °C. In order to further study the synthesis of pure phase nanocrystalline, we used hydrothermal method to refine the precursor materials and combined with molten salt method to control the nucleation growth in this paper. The results show that the hydrothermal-molten salt method can synthesize the pure phase ZST and reduce the temperature to 1000 °C even further. To our knowledge, no such studies on ZST powders with around nano crystalline morphology prepared by hydrothermal-molten salt method have ever been reported. In addition, we preliminarily explored the properties of ZST nano crystalline powders in UV catalysis and UV shielding to expand its applications.

2 Experimental

2.1 Experimental process

Analytical grade $ZrOCl_2{\cdot}8H_2O$ (99.0%), $SnCl_4{\cdot}5H_2O$ (99.0%), TiO_2 (99.0%), NaCl (99.5%), KCl (99.5%) and NaOH (99.0%) were used to synthesize ZST particles. The experimental parameters for synthesis of ZST powders are shown in Table 1 (A1 and E1 represents the sample synthesized by solvothermal method. H1 represents the sample synthesized by hydrothermal method, HS1 refers to the sample synthesized by hydrothermal-solid state method, HM series refer to the process parameters of hydrothermal-molten salt method). The preparation of ZST particles by hydrothermal-molten salt method has been carried out in two steps. The experimental flow chart is shown in Figure 1. The first step displays the hydrothermal method to obtain the precursor powders. First of all, the $ZrOCl_2{\cdot}8H_2O$, $SnCl_4{\cdot}5H_2O$ and TiO_2 were weighed according to the stoichiometry ratio of ZST, and were mixed with deionized water into a certain concentration solution. The pH of the solution was adjusted with NaOH. Then the mixed solution was placed in a hydrothermal reactor at 200 °C for 10 h. Finally, the precursor powders was obtained by repeatedly washing the precipitate with water bath for 3-5 times. The second step is to obtain the final product by molten salt method. The NaCl and KCl were weighted by mass ratio in 1:1, 1:3 and 3:1, respectively, as the compound molten salt. As shown in Figure 1, firstly the precursor powders and compound molten salt (by the mass ratio of 1:4) were mixed by balling milling with zirconia ball in deionized water for 4 h. And then, the dried mixture was put into corundum crucible and calcined at 950 °C and 1000 °C respectively, and the holding time was 4 h. Finally, the desired particles were separated from the solidified salt by washing several

Table 1 The experimental parameter of preparing ZST powders

Synthesis method	Sample numbers	Reaction solvent	PH	Calcination temperature	Molten salt constituent(mol %) NaCl: KCl
Solvothermal method	A1	Acetylacetone	Unadjusted	No sintering	None
Solvothermal method	E1	Ethylene glycol	Unadjusted	No sintering	None
Hydrothermal method	H1	Deionized water	Unadjusted	No sintering	None
Hydrothermal-solid state method	HS1	Deionized water	9	1100 °C	None
Hydrothermal-molten salt method	HM1		5	1000 °C	1: 1
	HM2	Deionized water			1: 3
	HM3				3: 1
	HM4		7	1000 °C	1: 1
	HM5	Deionized water			1: 3
	HM6				3: 1
	HM7		9	1000 °C	1: 1
	HM8	Deionized water			1: 3
	HM9				3: 1
	HM10		11	1000 °C	1: 1
	HM11	Deionized water			1: 3
	HM12				3: 1
	HM13	Deionized water	9	950 °C	1: 1

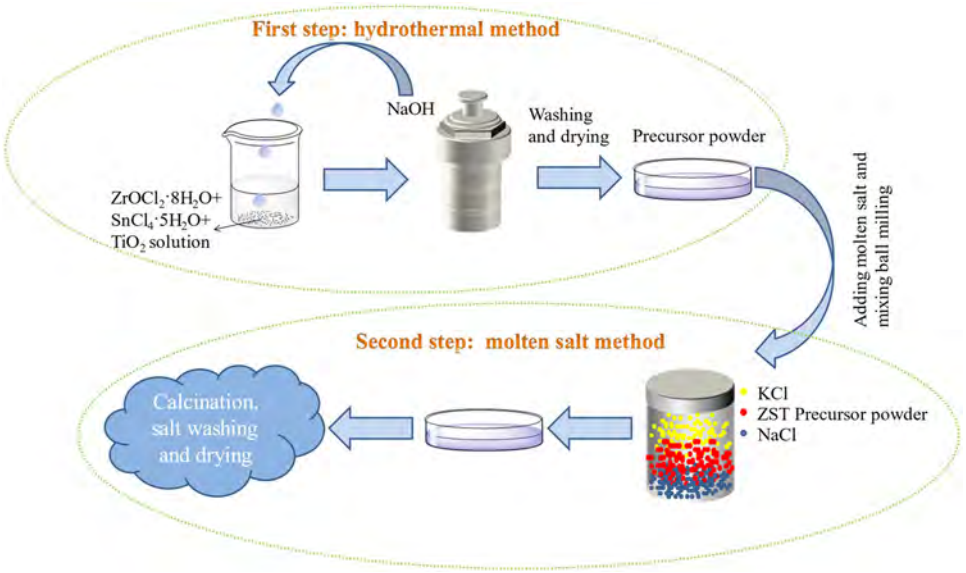

Fig. 1 Process flow chart of ZST powder prepared by hydrothermal-molten salt method

times in deionized water to ensure complete removal of the excess NaCl and KCl salts.

2.2 Characterization techniques

The phase analysis of samples was investigated by using X-ray diffractometry (XRD, XRD-6100, Shimadzu, Japan) with CuKα radiation ($\lambda = 0.15406$ nm). The scanning angle is 10° to 80° and the scanning speed is 5°/min. The morphologies of samples and selected-area electron diffraction (SAED) were analyzed by micro-electron-beam diffraction linked to transmission electron microscopy (TEM, JEM-2100, Jeol, Japan). Ultraviolet visible spectrophotometer (UV-759CRT, Shanghai, China) was used to measure the absorbance of methylene blue solution at the maximum absorption wavelength.

2.3 Evaluation of photocatalytic performance

The UV photocatalytic activity of $(Zr_{0.8},Sn_{0.2})TiO_4$ powders were tested with methylene blue (MB) as the target degradation substance by using 300 W xenon lamp as light source with 200-400 nm UVREF. The specific process of photocatalytic degradation experiment was as follows: accurately weighed 2 mg of MB dye into an erlenmeyer flask containing 200 mL of deionized water, shake it up preparing a dye solution with a concentration of 10 mg/L. And then 20 mL of MB solution and 20 mg ZST powders were added to a 50 mL beaker under dark light by magnetic stirring for 30 min to disperse evenly and achieve adsorption-desorption balance. Subsequently, the suspension was then poured into a quartz reactor irradiated under ultraviolet light (the liquid level was about 20 cm from the light source), and the temperature of the entire photocatalytic reaction process was controlled constantly by a circulating water cooling system. 4 mL of solution were taken into the centrifuge tube every 20 min, centrifuged for 3 min (speed rate at 2000 r/min), and the supernatant without catalyst powder was taken as a sample to characterize the photocatalytic degradation efficiency.

3 Results and discussion

The XRD patterns of samples synthesized by different synthesis methods are exhibited in Figure 2. It can be observed that only TiO_2 (anatase), ZrO_2 and SnO_2 are detected in A1 and E1 samples. Although a small amount of ZST phase is formed in H1 samples, lots of TiO_2 (anatase), ZrO_2 phase are detected. This means that the single hydrothermal reaction cannot meet the conditions for the completely synthesis of ZST phase. The ZST phase is the primary crystal phase in the HS1 samples, but the diffraction peaks of ZrO_2 and $Na_2Ti_6O_{13}$ are observed. The patterns show that the HM7 samples have an α-PbO_2 orthorhombic structure (which can be indexed as ZST, JCPDS 81-2214) without evidence of any additional phase. Compared with the hydrothermal-solid state method (HS1), the hydrothermal-molten salt method has excellent advantages to obtain high crystalline and high purity powders, and the synthesis temperature can be reduced to 1000 °C. It was attributed to that liquid molten salt can enhance the fluidity of reaction components in the liquid phase, accelerating the diffusion rate between ions. This provides a basis for the development of high-performance low-temperature sintering of ZST ceramics.

In order to explore a better synthesis process of hydrothermal-molten salt method, the influences of the pH of solvent system, the calcinations temperature and the ratio of composite molten salt on the phase composition and crystalline morphology were further studied.

Figure 3 illustrates the X-ray diffraction patterns of the samples synthesized by hydrothermal-molten salt method under different pH values. The major crystal phase of all samples matches with standard card (JCPDS 81-2214) of ZST. But there is still a small amount of impurity phase. With the increase of pH value, the intensity of ZST main crystal phase increases and the peak shape becomes sharp, which indicate that the crystal growth tends to be complete and the crystallinity is improved. The pH continues to rise to 11, the diffraction peak intensity becomes weaker and the peak shape widen, and the $Na_2Ti_6O_{13}$ phase appears. This demonstrates that excess alkalinity is not conducive to the synthesis of ZST powders, and causes the crystallinity of

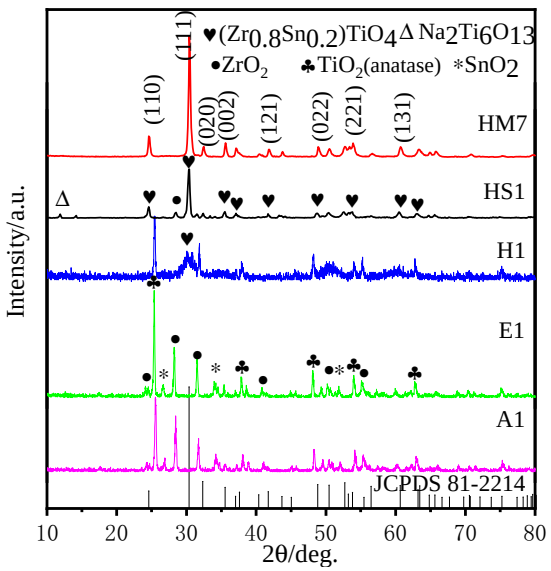

Fig. 2 XRD patterns of samples synthesized by different methods

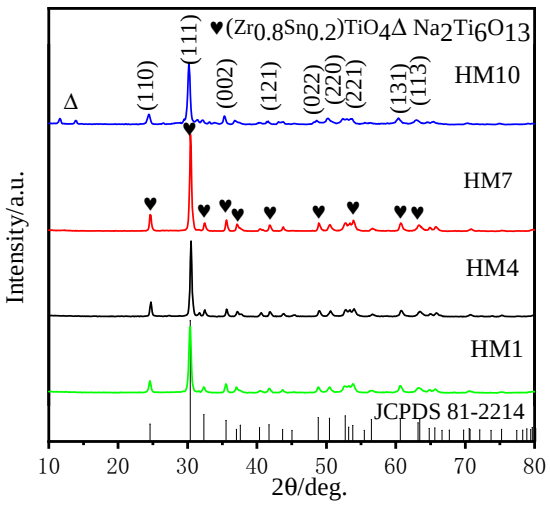

Fig. 3 XRD patterns of the samples synthesized by hydrothermal-molten salt method under different pH values

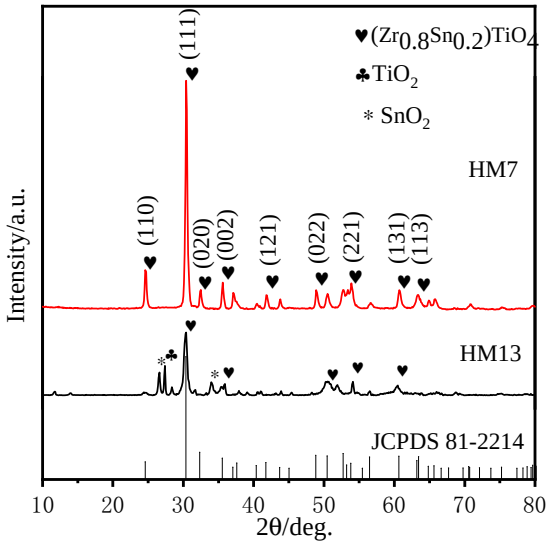

Fig. 4 XRD patterns of synthesized samples at different calcination temperatures for 4 h

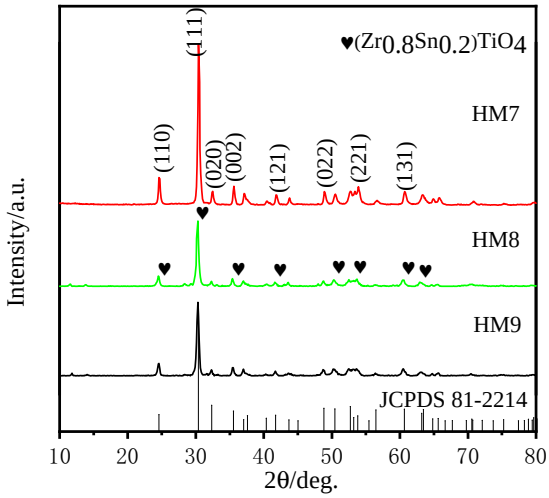

Fig. 5 XRD patterns of samples synthesized with different proportion of molten salt

ZST to decrease. According to the Scherer formula $D = K\lambda/B\cos\theta$ (K is 0.89, λ is 0.15405 nm), the average particle sizes of samples HM1, HM4, HM7 and HM10 are calculated to be 24.50 nm, 29.34 nm, 30.44 nm, 23.40 nm, respectively. It can be seen that pH plays an important role in regulating the growth of ZST crystals.

Figure 4 reveals XRD patterns of ZST powders calcined at different temperatures. It can be seen that TiO_2 (Rutile phase) and SnO_2 impure phase are detected in HM13 samples synthesized at 950 °C. As the temperature increasing from 950 °C to 1000 °C, the diffraction peaks are identified to be pure phase ZST (HM7 samples), and no other obvious impurities can be found. The appearance of TiO_2 (rutile phase) and SnO_2 is due to the insufficient driving force of low sintering temperature on the synthesis of pure phase.

Figure 5 demonstrates the XRD diffraction pattern of samples synthesized with different molten salt ratios. The diffraction peaks of the all samples correspond to α-PbO_2 orthorhombic structure in agreement with the standard card (JCPDS 81-2214). The sharp diffraction peaks of the ZST powders with molten salt ratio of 1:3 and 3:1 are wider and unsmooth, indicating that the powders has poor crystallinity. The sharp diffraction peaks show that well crystallized ZST crystal can be obtained when the ratio of molten salt is 1:1. The eutectic point of the two phases is 657 °C for the NaCl-KCl composite molten salt with the ratio of 1:1, the proper liquid phase content forms and accelerates the mass transfer and diffusion rate between ions, thereby profiting the nucleation and growth of the ZST crystal phase. However, whether the excess NaCl or the excess KCl, insufficient liquid phase content is caused, the ion reaction and the growth of the ZST crystal are affected.

The TEM micrographs, SADE patterns and HRTEM photos of the HS1 samples obtained at 1100 °C are depicted in Figure 6. It can be observed that the specimen shows the rod-like crystalline morphology with grain diameter about 200 nm. However, the shape is irregular, with small particles on the edge. Figure 6d shows the selected area electron diffraction pattern of the red circle part in Figure 6b, indicating that the ZST has a single crystal structure. Therefore, it is speculated that the long rod-shaped structure of ZST is formed by the preferred growth of small particles via dissolution-precipitation, which illustrates that the preferred growth of crystal can be achieved by prolonging the holding time and changing the crystal growth system. Figure 6f reveals an enlarged view of the selected area of Figure 6e. The HRTEM of HS1 samples was measured by Digital Micrograph software, the distance between lattice frings is 0.275 nm, which is consistent with the (020) plane of orthorhombic ZST. However, the stripes between the crystal surfaces are not clear, which indicates that the crystallinity of the crystals is poor. The single crystal electron diffraction pattern in Figure 6d has been calculated and calibrated. The crystallization indexes are (111), (100), and (211) respectively, and its crystal belt axis direction is confirmed to be $[01\bar{1}]$.

Figure 7 illustrates the TEM micrographs, SADE patterns and HRTEM photos of the HM7 sample obtained at 1000 °C. The ZST crystalline powders prepared by hydrothermal-molten salt method are indicative of a short rod-like structure with a regular morphology and obvious boundaries. After careful observation of Figure 7, it can be observed that the surface of the single crystal rod is smooth, and there is no deposition of small particles as shown in Figure 6, which indicates that crystal growth is complete. Compared with hydrothermal-solid state method (HS1), the

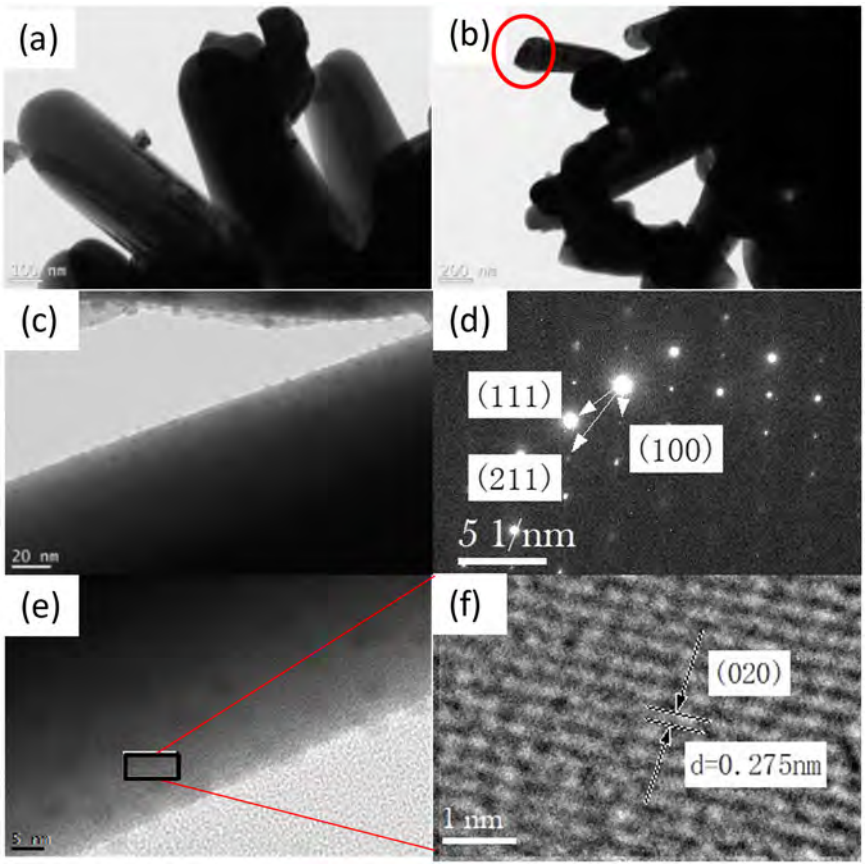

Fig. 6 TEM micrographs ((**a**), (**b**),(**c**)), SADE images ((**d**)) and HRTEM photos ((**e**),(**f**)) of ZST nanocrystal particles prepared by hydrothermal-solid state method

grain size of the rod is significantly reduced to 50–60 nm in diameter and 500–600 nm in length, and the crystal has uniform morphology and good dispersion. Thus, the hydrothermal-solid state method is based on the migration of grain boundaries and then swallows each other to grow up, showing that the larger particles grow, the smaller the particles disappear. It can be inferred that the crystal synthesized has a certain preferred orientation and grows in rod shape in hydrothermal system. The molten salt medium plays an important role in regulating the morphology growth process [27], which makes the grain growth finer. This also greatly increases the surface energy of grain, which helps to provide sintering powders for the follow-up. The results suggest that hydrothermal-molten salt method is easier to synthesize high purity and high activity nano powders at low temperature, which is consistent with the XRD analysis results. Figure 7f is an enlarged view of the selected area of Figure 7e. It can be seen that the crystal plane stripes are clear, indicating that ZST crystal has well crystallinity in the HM7 samples. The lattice frings with an interval of approximately 0.292 nm were visible and accordance with (111) plane. Figure 7d is electron diffraction pattern from the selected areas in Figure 7b, indicated by red circle. It can be observed from the figure that the diffraction spots are uniformly arranged and distributed, which is a typical single crystal electron diffraction pattern. The crystal indexes are (101), (020) and (121) via measurement and calibration, and the axis direction of crystal belt is $[\bar{1}01]$, which is consistent with the crystal surface index of ZST structure. It shows that ZST rod-like crystal has the characteristics of preferentially grown single crystal, and can be used as start materials for preparing ZST textured ceramics.

In order to expand the application field of $(Zr_{0.8},Sn_{0.2})TiO_4$ nano powders, the photocatalytic performance and UV shielding property were characterized by UV-visible spectrophotometer.

Figure 8 shows the degradation curve of methylene blue using ZST powders synthesized by hydrothermal-molten salt method as photocatalyst. It can be observed from the figure that all synthesized ZST powders have certain degradation effect on methylene blue solution. Within a certain range, the absorbance decreases with the increase of pH values, and the maximum degradation rate is 64% at pH = 9. But when the pH continues to increase to 11, the degradation rate is greatly reduced to only 25.7%. According to the analysis of XRD pattern in Figure 3, the half-height width of diffraction peak gradually decreases

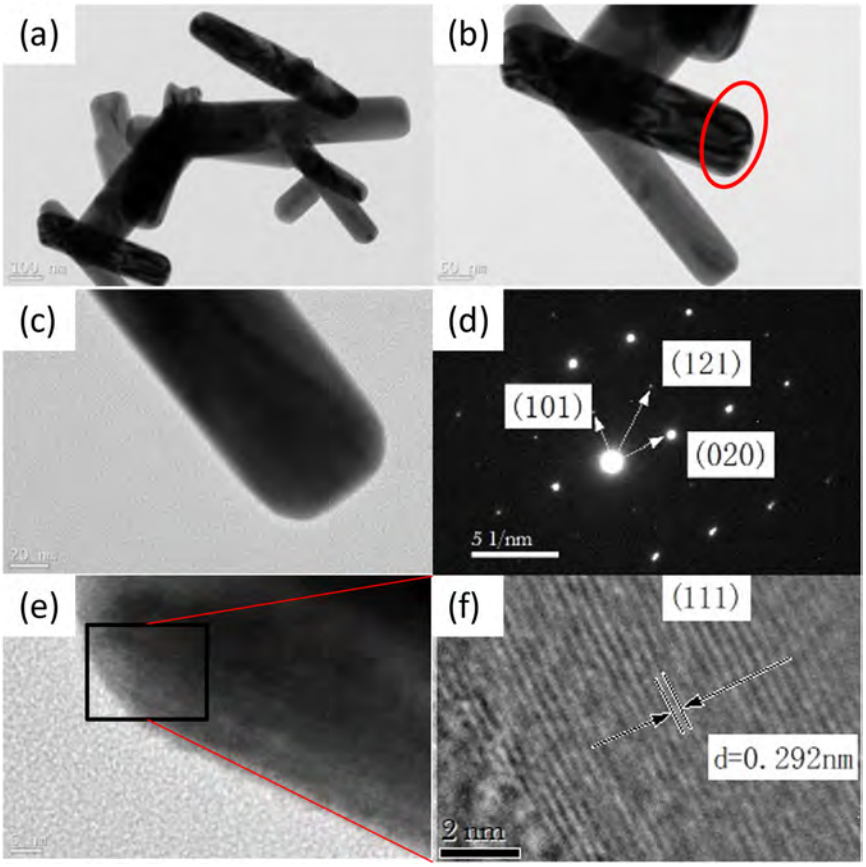

Fig. 7 TEM micrographs ((**a**), (**b**),(**c**)), SADE images ((**d**)) and HRTEM photos ((**e**),(**f**)) of ZST nanocrystal particles prepared by hydrothermal-molten salt method

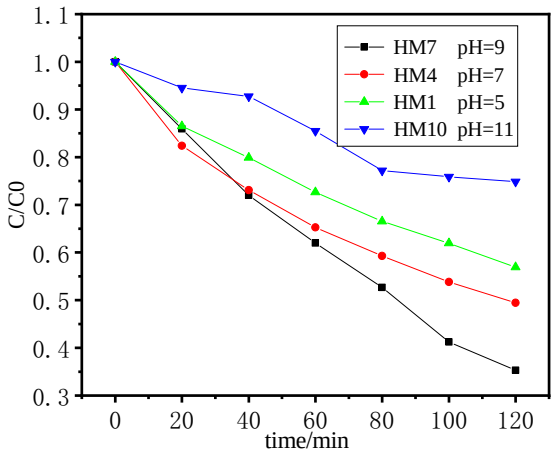

Fig. 8 The degradation curve of methylene blue using ZST powders synthesized by hydrothermal-molten salt method as photocatalyst

with increasing the pH, which indicates that the crystallization is more complete and the defects are reduced. However, as the pH value is increased to 11 continually, the half-height width of diffraction peak suddenly increases, indicating that the crystal growth is incomplete and the defects are increased. The more defects in the crystal, the easier it is for electrons and holes to recombine, which will lead to the degradation of photodegradation performance. In addition, the change of pH has an effect on the agglomeration degree and specific surface area of the powders. with the increase of pH, the dispersion and specific surface area of the powders increase, and the catalytic degradation activity of methylene blue is enhanced. However, the continued increase of the pH value leads to agglomeration of powders, which reduces the degradation rate and catalytic performance.

The first-order reaction kinetics fitting of methylene blue solution is shown in Figure 9. It can be seen that the fitted curve is linear. According to the equation ($\ln C/C0 = -kt$), it can be concluded that the interface reaction rates K1, K2, K3, and K4 correspond to different pH (5, 7, 9, 11) respectively. It can be seen that the reaction rate of HM7 samples is the highest, which indicates that it has high degradation rate and strong catalytic activity. It can prove the conclusion of the aforementioned photocatalytic degradation.

As shown in Figure 10a, the absorption edges of all samples are almost the same in the ultraviolet region. Correspondingly, Figure 10b reveals that the optical band gaps of ZST are determined from the Kubelka Munk and Tauc plot by the plots of $(Ahv)^2$ versus (hv). It can be seen that the band gaps of all samples are between 3.4 eV and 3.5 eV, which indicates that the optical absorption and the

separation efficiency of photogenerated electron hole pairs are similar [28]. Combined with the analysis of Figure 8 and Figure 9, it can be found that the optical band gap has almost no effect on the photocatalytic degradation performance.

Ultraviolet is a kind of electromagnetic wave with short wavelength. The wavelength range is between 200 and 400 nm. It can be divided into three bands: UVA (320–400 nm), UVB (280–320 nm) and UVC (200–280 nm) [29, 30]. The wavelength of sunlight reaching the ground is 290-3000 nm. Therefore, short wave ultraviolet (UVC) cannot reach the ground due to the obstruction of ozone layer, only UVA and UVB can reach the ground [31, 32]. Figure 11 shows the change of absorbance with wavelength. It can be seen that the ZST nano powders synthesized by hydrothermal-molten salt method has good absorption properties of ultraviolet light. The absorption curve of UVA (320–400 nm) exhibits a step shape, which broadens the UV absorption region. In the UVB section, the absorption shows the strongest peak, corresponding to the wavelength of about 330 nm, which is basically the boundary between UVA and UVB. It can be observed from the figure that HM7 samples exhibits the best absorption properties of ultraviolet light. The pH increases to 11, the UV shielding effect of HM10 samples is significantly reduced, which indicates that the ZST powders with a large specific surface area is more conductive to UV absorption.

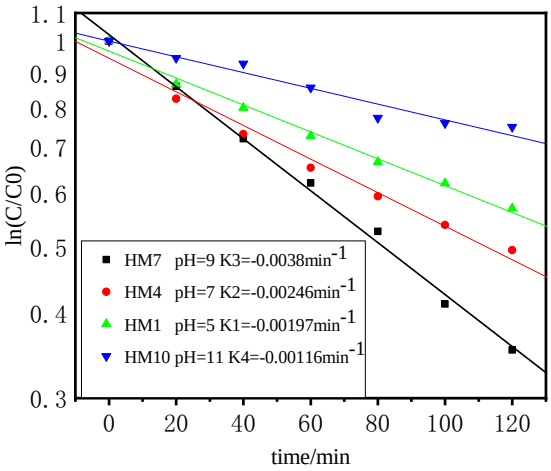

Fig. 9 *t*–ln (C/C_0) relation curve of methylene blue degraded by ZST powders

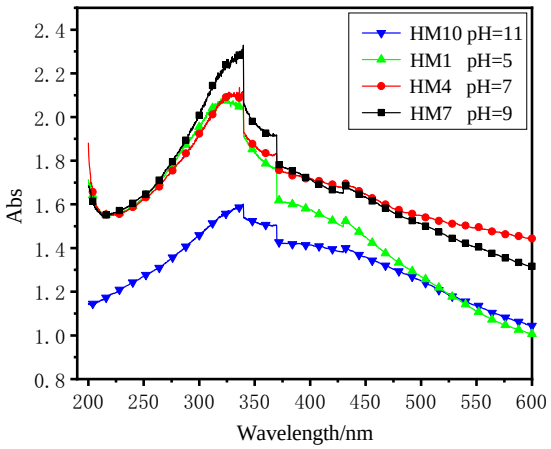

Fig. 11 Absorbance of ZST powder with different pH value to UV light

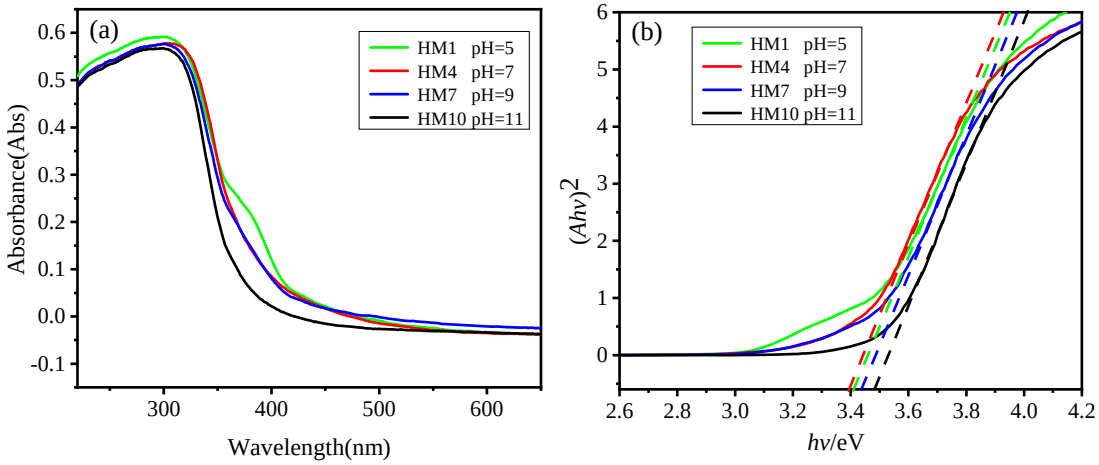

Fig. 10 UV-vis diffuse reflectance spectra (DRS) (**a**) and the Kubelka Munk and Tauc plot (**b**) of ZST powders with different pH prepared by hydrothermal-molten salt method. Absorbance of ZST powder with different pH value to UV light

4 Conclusions

The pure phase ZST nano crystals were prepared by hydrothermal-molten salt method at 1000 °C. The synthesized temperature of single phase ZST is lower and the crystal growth is more complete compared with the solid state reaction. The rod-like crystalline grain are evenly distributed with a diameter of about 50–60 nm and can be used as start materials for preparing ZST textured ceramics. The ZST nano crystal has a certain photocatalytic effect and good UV shielding performance.

Acknowledgements The work was supported by Natural Science Foundation of China (51602252) and National Key Basic Research and Development Project Subproject (2017YFC0703204).

Compliance with ethical standards

Conflict of interest The authors declare no competing interests.

Publisher's note Springer Nature remains neutral with regard to jurisdictional claims in published maps and institutional affiliations.

References

1. Yang RY, Weng MH, Kuan H (2009) TEM observation of liquid phase sintering in V_2O_5 modified $(Zr_{0.8},Sn_{0.2})TiO_4$ microwave ceramics. Ceram Int 35:39–43
2. Lyu XS, Li LX, Sun H, Zhang S, Li S (2016) High-Q microwave dielectrics in wolframite magnesium zirconium tantalate ceramics. Ceram Int 42:2036–2040
3. Zhang Y, Ding SH, Li C, Song TX, Zhang YC (2020) Bond analysis of novel $MnZrTa_2O_8$ microwave dielectric ceramics with monoclinic structure. J Mater Sci 55:8491–8501
4. Bafrooei HB, Feizpour M, Sayyadi-shahraki A, Song KX (2020) High-performance $ZnTiNb_2O_8$ microwave dielectric ceramics produced from $ZnNb_2O_6$-TiO_2 nano powders. J Alloy Compd 834:155082
5. Guo J, Zhou D, Wang H, Yao X (2011) Microwave dielectric properties of (1-x)$ZnMoO_4$-xTiO_2 composite ceramics. J Alloy Compd 509:5863–5865
6. Zhou HF, Tan X, Huang J, Wang N, Fan GC, Chen XL (2017) Phase structure, sintering behavior and adjustable microwave dielectric properties of $Mg_{1-x}Li_{2x}Ti_xO_{1-2x}$ solid solution ceramics. J Alloy Compd 696:1255–1259
7. Xiang HC, Fang L, Fang WS, Tang Y, Li CC (2017) A novel low-firing microwave dielectric ceramic $Li_2ZnGe_3O_8$ with cubic spinel structure. J Eur Ceram Soc 37:625–629
8. Zhang Y, Ding SH, Song TS, Zhang YC (2019) Microwave dielectric properties of temperature stable MO-ZrO_2-Ta_2O_5 ceramics. J Alloys Compd https://doi.org/10.1016/j.jallcom.2019.05.251
9. Yang RY, Weng MH, Su YK, Ye CS, Wu HW (2009) Effect of annealing temperatures on microstructure of $(Zr_{0.8}Sn_{0.2})TiO_4$ thin films grown by a sol–gel process. J Alloy Compd 471:511–514
10. Wang X, Zou ZY, Song XQ, Lei W, Zhong LW (2018) The effects of dispersants on sinterability and microwave dielectric properties of $(Zr_{0.8}Sn_{0.2})TiO_4$ ceramics. Ceram Int 44:14990–4994
11. Wang LZ, Wang LX, Wang ZF, Huang BY, Fu ZX (2016) Effect of ZnO/Er_2O_3 addition on microwave properties of $(Zr_{0.8}Sn_{0.2})TiO_4$ ceramics. J Mater Sci Mater Electron 27:3929–3933
12. Kim DJ, Hahn JW, Han GP, Lee SS, Choy TG (2000) Effects of Alkaline-Earth-Metal addition on the snterability and microwave characteristics of $(Zr,Sn)TiO_4$ dielectrics. J Am Ceram Soc 83:1010–1012
13. Jiang HT, Zhai JW, Zhang MW, Yao X (2012) Enhanced microwave dielectric properties of $Ba_{0.40}Sr_{0.60}TiO_3$–$Zr_{0.80}Sn_{0.20}TiO_4$ composite ceramics. J Mater Sci 47:2617–2623
14. Vahabzadeh S, Golozar MA, Ashrafizadeh F (2011) Effect of annealing on microstructure of CuO-doped $(Zr_{0.8}Sn_{0.2})TiO_4$. J Alloy Compd 509:1129–1132
15. Sun QL, Zhou HQ, Luo XF, Hu LS, Ren LC (2016) Influence of La_2O_3/SrO doping of $(Zr_{0.8}Sn_{0.2})TiO_4$ ceramics on their sintering behavior and microwave dielectric properties. Ceram Int 42:12306–12311
16. Bhuyan RK, Kumar TS, Goswami D, James AR, Pamu D (2013) Liquid phase effect of La_2O_3 and V_2O_5 on microwave dielectric properties of Mg_2TiO_4 ceramics. J Electroceram 31:48–54
17. Wang LZ, Wang LX, Wang ZF, Huang BY, Zhang QT, Fu ZX (2015) Effect of sintering aid ZnO-CeO_2 on dielectric properties of $(Zr_{0.8}Sn_{0.2})TiO_4$ ceramics. J Mater Sci Mater Electron 26:9026–9030
18. Pamu D, Rao GLN, Raju KCJ (2011) Low temperature processing of $(Zr_{0.8}Sn_{0.2})TiO_4$ ceramics with improved Q factor. J Alloy Compd 509:9289–9295
19. Sun QL, Zhou HQ, Zhu HK, Qi HQ, Hu LS, Yue ZX (2016) Sintering behavior and microwave dielectric properties of Y_2O_3-ZnO doped $(Zr_{0.8},Sn_{0.2})TiO_4$ ceramics. J Mater Sci Mater Electron 27:7750–7754
20. Olhero SM, Kaushal A, Ferreira JMF (2014) Fostering the properties of $(Zr_{0.8}Sn_{0.2})TiO_4$ (ZST) ceramics via freeze granulation without sintering additives. Rsc Adv 4:48734–48740
21. Arantes VL (2012) Sintering and microwave properties of zirconium tin titanate doped with select oxides. J Mater Eng Perform 21:1777–1784
22. Heiao YC, Wu L, Wei CC (1988) Microwave dielectric properties of $(ZrSn)TiO_4$ ceramic. Mat Res Bull 29:1687–1692
23. Yu HG, Shen ZH, Bao DY, Xiong ZX (2004) Preparation of ZST microwave ceramic powder by hydrothermal method. J Funct Mater 35:3152–3154
24. Wu JQ, Guo HF, Cao Y (2017) Preparation of SnO_2-ZnO/ZST ceramics by precipitation method and its Q value. J Ceram 38:217–220
25. Ho YS, Chen TS, Yang WD (2010) The effect of tin precursors on the formation of $(Zr_{0.8}Sn_{0.2})TiO_4$ nano-powder by sol gel process. J Sol-Gel Sci Technol 53:613–618
26. Ge HY, Hou YD, Yang JF, Zhu MK, Wang H, Yan H (2013) Fabrication and properties of $Na_{0.9}K_{0.1}NbO_3$ nanostructures by molten salt synthesis. Powder Technol 246:144–147
27. Li C, Chiu C, Desu SB (1991) Formation of lead niobates in molten salt systems. J Am Ceram Soc 74:302–307
28. Yan W, Liu XC, Hou S, Wang X (2019) Study on Micro-nanocrystalline Structure Control and Performance of $ZnWO_4$ photocatalysts. Catal Sci Technol 9:1141–1153
29. Wang Y, Zuo SX, Li XZ, Liu WJ, Xu R, Zhong J, Yao C (2020) Ultrafine TiO_2 Rheological properties and UV protection properties in silicone oil. China Surfactant Deterg Cosmetics 50:112–117
30. Kurz W, Yetisen AK, Kaito MV, Fuchter MJ, Jakobi M, Elsner M, Koch AW (2020) UV-sensitive wearable devices for colorimetric monitoring of UV exposure. Adv Opt Mater 8:1901969
31. Kockler J, Oelgemöller M, Robertson S, Glass BD (2012) Photostability of sunscreens. J Photoch Photobio C 13:91–110
32. Reinosa JJ, Leret P, Alvarez-Docio CM, Campo A, Fernandez JF (2016) Enhancement of UV absorption behavior in ZnO–TiO_2 composites. J Bol Soc Esp Ceram V 55:55–62